

[REDACTED]

WIND-TUNNEL INVESTIGATION OF AERODYNAMIC LOAD DISTRIBUTION
ON A VARIABLE-WING-SWEEP FIGHTER AIRPLANE WITH
A NASA SUPERCRITICAL AIRFOIL*

By James B. Hallissy and Charles D. Harris
Langley Research Center

SUMMARY

Wind-tunnel tests have been conducted at Mach numbers of 0.85, 0.88, and 0.90 to determine the aerodynamic load distribution for the 39° swept-wing configuration of a variable-wing-sweep fighter airplane with a NASA supercritical airfoil. Chordwise pressure distributions were measured at two wing stations. Also measured were the overall longitudinal aerodynamic force and moment characteristics and the buffet characteristics. The analysis indicates that localized regions of shock-induced flow separation may exist on the rearward portions of the supercritical wing at high subsonic speeds, and caution must be exercised in the prediction of buffet onset when using variations in trailing-edge pressure coefficients at isolated locations.

INTRODUCTION

At high subsonic Mach numbers, localized regions of supersonic flow exist on the upper surface of an airfoil. These localized regions of supersonic flow are usually terminated by a shock wave, bringing on the phenomenon of boundary-layer separation and precipitous drag rise. In addition, buffet onset is usually associated with boundary-layer separation.

Two-dimensional wind-tunnel investigations of recently developed supercritical airfoils (refs. 1 to 3) have indicated that substantial improvements in aircraft performance at high subsonic speeds might be achieved by shaping the airfoil to minimize shock-induced separation on the upper surface. The supercritical-airfoil concept utilizes proper shaping of the pressure distribution to control boundary-layer separation. This is accomplished by flattening the midchord region of the airfoil upper surface and increasing its camber near the trailing edge, which results in a more uniform supersonic flow over the upper surface and greatly reduced shock strength and boundary-layer separation.

*Title, Unclassified.

[REDACTED]

[REDACTED]

In order to further substantiate the performance gains of the two-dimensional-wing concept, a program was initiated by NASA to investigate the aerodynamic characteristics of a variable-wing-sweep fighter airplane model incorporating the supercritical airfoil. The results of this investigation, reported in reference 4, indicated substantial improvements in such performance parameters as cruise Mach number, range factor, and buffet onset when compared to the same model with a conventional airfoil.

Additional tests have been conducted to measure the wing pressure distribution and the buffet characteristics of the above-mentioned fighter aircraft model at selected test conditions. The total aerodynamic forces and moments acting on the model were also measured and these results are included. This investigation was limited to a configuration having the wing leading-edge sweep angle fixed at 39° . The tests were conducted in the Langley 8-foot transonic pressure tunnel at Mach numbers of 0.85, 0.88, and 0.90, at angles of attack from 3° to 10° , and a Reynolds number of approximately 2.07×10^6 based on a wing mean geometric chord of 11.483 cm (4.521 in.).

SYMBOLS

The model aerodynamic data presented herein are referenced to the body-axis system except for lift and drag which are referred to the stability-axis system. The wing section pitching-moment coefficients are referenced to the quarter-chord line of the wing in the 26° sweep configuration. All other data are referenced to a moment center on the model reference line located at station 55.756 cm (21.951 in.) which corresponds to $0.45\bar{c}$ for $\Lambda = 16^\circ$. All coefficients are nondimensionalized with respect to the geometry of the model having a wing leading-edge sweep angle of 16° .

Values are given in both SI and U.S. Customary Units. The measurements and calculations were made in U.S. Customary Units.

C_A	axial-force coefficient, $\frac{\text{Axial force}}{qS}$
C_D	drag coefficient, $\frac{\text{Drag}}{qS}$
C_L	lift coefficient, $\frac{\text{Lift}}{qS}$
C_m	pitching-moment coefficient, $\frac{\text{Pitching moment}}{qS\bar{c}}$
C_p	pressure coefficient, $\frac{p - p_\infty}{q}$

$C_{p,te}$	pressure coefficient at trailing edge
c	local wing chord, cm (in.)
\bar{c}	wing mean geometric chord, 11.483 cm (4.521 in.)
c_m	section pitching-moment coefficient, $\int_0^{1.0} (C_{p,l} - C_{p,u}) \left(0.25 - \frac{x}{c}\right) d\left(\frac{x}{c}\right)$
c_n	section normal-force coefficient, $\int_0^{1.0} (C_{p,l} - C_{p,u}) d\left(\frac{x}{c}\right)$
M	free-stream Mach number
M_p	rms output of wing bending gage, m-N (in.-lb)
p	local static pressure at a point on the airfoil, N/m^2 (lb/ft ²)
p_∞	free-stream static pressure, N/m^2 (lb/ft ²)
q	free-stream dynamic pressure, N/m^2 (lb/ft ²)
S	wing area including fuselage intercept, 846 cm ² (0.911 ft ²)
x	streamwise distance aft of the wing leading edge, cm (in.)
α	angle of attack, referred to model reference line, deg
η	ratio of the distance outboard from the wing pivot station to the distance between the pivot station and the wing tip (fig. 5)
Λ	leading-edge sweep of outboard wing panel, deg

Subscripts:

l	wing lower surface
u	wing upper surface

APPARATUS AND PROCEDURES

Model Description

The general arrangement of the 1/24-scale model utilized for this investigation is shown in figure 1 and photographs of the model are presented as figure 2. The model has a variable-sweep wing with the pivot located longitudinally at model station 51.610 cm (20.319 in.) and laterally 7.440 cm (2.929 in.) outboard of the model plane of symmetry. Details of the wing planform are presented in figure 3. The portion of the trailing edge of the wing bounded by span stations 10.579 cm (4.165 in.) and 17.043 cm (6.710 in.) and the 65-percent chord line was modified as shown to allow the wing to clear the engine ducts when the leading-edge sweep was 72.5° . A wing dihedral angle of 1° was incorporated outboard of span station 8.839 cm (3.480 in.).

The wing coordinates were similar to those of supercritical wing C described in reference 4, and incorporated a uniform twist about the 26.146-percent chord line such that the incidence at the tip was 6° more negative than at the pivot. A sketch of a typical airfoil section is shown in figure 4. For the present investigation the wing leading-edge sweep angle was fixed at 39° and the incidence of the wing chord plane at the pivot was -3° (leading edge down) relative to the model reference line.

The horizontal tails consisted of biconvex airfoil sections and were mounted with a deflection of -4° (leading edge down) during this investigation. The vertical tail consisted of 3.2-percent-thick modified biconvex airfoil mounted in the model plane of symmetry. Twin ventral fins were mounted on the lower aft fuselage and canted outward 30° from the model plane of symmetry.

Tunnel

The investigation was made in the Langley 8-foot transonic pressure tunnel. The test section in this tunnel is square in cross section with the upper and lower walls axially slotted to permit changing the test-section Mach number continuously from 0 to over 1.20. This facility has controls that allow independent variation of Mach number, stagnation pressure, temperature, and specific humidity. Additional information about the facility may be obtained from reference 5.

Boundary-Layer Transition

Transition was fixed on the upper and lower surfaces of the outboard wing panels to simulate the full-scale Reynolds number boundary-layer separation characteristics. From consideration of the techniques discussed in references 6 and 7 and from use of the fluorescent-oil film technique (ref. 8) to observe boundary-layer flow patterns, the

[REDACTED]

boundary-layer trips on the upper surface were located at about 5-percent chord at the wing-glove juncture and angled rearward to intersect the 42-percent chord line at a point 15.2 cm (6.0 in.) outboard of the wing-glove juncture measured along the span. The trip continued from this point to the tip along the 42-percent-chord line. The lower-surface trip was located along the 42-percent-chord line from the wing-glove juncture to the wing tip. The trips were 0.127 cm (0.05 in.) wide and consisted of No. 120 carborundum grains set in a plastic adhesive. Similar boundary-layer trips were also placed on the fuselage 3.8 cm (1.5 in.) aft of the nose using No. 120 carborundum grains and 1.0 cm (0.4 in.) aft of the leading edges of the wing glove, inlet nacelles, ventral fins and horizontal and vertical tails using No. 150 carborundum grains.

Measurements

Wing surface pressure measurements were obtained by means of electrically actuated differential-pressure scanning units mounted in the fuselage nose cavity. Flush-mounted surface static-pressure orifices were located in chordwise rows at 30- and 70-percent stations (measured outboard from the wing pivot point, see fig. 5) with the wings at a leading-edge sweep angle of 26° . Rearward facing orifices were included in the wing trailing edge to measure the pressure at the trailing edge. The orifice locations are listed in table I and sketched in figure 5. Section normal-force and pitching-moment coefficients were obtained by numerical integration (based on the trapezoidal method) of the local pressure coefficients measured at each orifice multiplied by an appropriate weighting factor (incremental area).

Overall static aerodynamic force and moment measurements were obtained by means of an electrical strain-gage balance located within the fuselage cavity.

The buffet information included herein was obtained by the wing-root bending-moment technique described in references 9 and 10. The wing gages were located in the position shown in figure 3 and consisted of four active strain gages forming a complete bending-moment bridge. The results as presented in this paper represent the average rms values of the fluctuating wing-root-bending moments integrated over a 45-sec sampling time.

The measurements were taken over an angle-of-attack range from about 3° to 10° at 0° sideslip for a wing leading-edge-sweep angle of 39° . Data were obtained at Mach numbers of 0.85, 0.88, and 0.90 and a constant free-stream Reynolds number of 2.07×10^6 based on the wing mean geometric chord ($\Lambda = 16^{\circ}$).

Corrections

Because of the high loads imposed on the model and the necessity of obtaining data at angles of attack where severe model buffeting occurred, a model-sting arrangement

[REDACTED]

[REDACTED]

was chosen in which the sting diameter was increased, by a tapered section, immediately aft of the model base. The wing pressure distributions, which were of primary importance in this investigation, are considered to be free of any interference effects. However, the close proximity of the sting taper to the model base produced a positive pressure field which affected the axial-force and pitching-moment measurements. The pitching-moment coefficients have been adjusted by incremental values determined from unpublished data of previous tests with a model sting which did not adversely affect the strain-gage data. The drag data have not been adjusted for this adverse pressure field and are therefore invalid insofar as absolute values are concerned. However, these drag data have been corrected for internal flow through the ducts (ref. 11) and adjusted to the condition of free-stream static pressure acting over the fuselage cavity and the nozzle-exit plug bases.

The measured angles of attack have been corrected for model support sting and balance deflections due to aerodynamic loads on the model.

RESULTS AND DISCUSSION

The principal emphasis in this investigation was on the pressure distribution over the supercritical wing at a Mach number of 0.90, a condition of primary interest to the military services. Consequently, a leading-edge-sweep angle of 39° , demonstrated in previous tests to result in the lowest drag at $M = 0.90$ (ref. 4), was utilized. Force and pressure measurements were also made at $M = 0.85$ and 0.88 with $\Lambda = 39^\circ$, although 39° is not the most satisfactory sweep angle at these Mach numbers.

The longitudinal aerodynamic and buffet characteristics of the model are presented in figures 6 and 7, and the chordwise pressure distributions at Mach numbers of 0.85, 0.88, and 0.90 are presented in figures 8 to 10. Also included in figures 8 to 10 are the section normal-force and pitching-moment coefficients at each angle of attack. A plugged orifice on the upper-surface outboard row ($\eta = 0.70$) at $\frac{x}{c} = 0.75$ required that the pressure distribution be arbitrarily faired between x/c values of 0.65 and 0.85. Similarly the data for the lower surface outboard row ($\eta = 0.70$) have been arbitrarily faired between x/c values of 0.45 and 0.65.

The chordwise pressure distributions generally show a rearward movement of the shock-wave location with increases in angle of attack and Mach number up to the point at which trailing-edge separation first occurs (as indicated by a rapid decrease in trailing-edge pressure coefficients summarized in fig. 7). With further increases in angle of attack, a forward displacement of the shock wave is noted. These shock pattern movements are better defined for the outboard station ($\eta = 0.70$) than for the inboard station

($\eta = 0.30$) where the situation is complicated by the development of a double-shock system at Mach numbers above 0.85. At these conditions the aft shock varies in the manner described. The forward shock wave, however, while moving aft with increasing angle of attack, shows little or no variation in position with changes in Mach number. (A detailed discussion of the variation of shock wave location with angle of attack and Mach number may be found in ref. 12.)

At high subsonic Mach numbers, where shock-induced separation may be present on only a localized rearward region of the supercritical wing, caution must be used in interpreting a rapid decrease in the trailing-edge pressure coefficients at isolated locations as an indication of buffet onset for the supercritical wing. This is illustrated in figure 7 where buffet characteristics are presented in the form of wing trailing-edge pressure coefficients, axial-force coefficients, and fluctuating wing-root bending moments. The angles of attack at which rapid decreases in $C_{p,te}$ occur at $\eta = 0.70$ for $M = 0.88$ and 0.90 correspond to the initial breaks in the axial-force coefficients which occur around 5° or 6° . Such breaks in the axial-force curves are associated with localized shock-induced separation over the trailing edge of the outboard wing region as indicated in the oil flow photograph in figure 11, taken at an angle of attack near 7° for $M = 0.90$ (the only Mach number for which oil flow photographs are available). However, the wing-root bending moments indicate that this localized shock-induced separation around 5° and 6° was not extensive enough to cause buffet onset. With further increases in angle of attack, the region of separated flow spreads until between 7° and 8° there is an indication of separation over the trailing edge of the inboard ($\eta = 0.30$) station. The point at which the inboard separation appears as a decrease in the trailing-edge pressure coefficient compares closely with the angle of attack for buffet onset as indicated by the wing-root bending moments. Flight-test data for a supercritical-wing research airplane (ref. 12), obtained subsequent to the present investigation, also indicate that the divergence of wing trailing-edge pressure coefficients is not a valid criterion for the prediction of buffet onset for supercritical-wing aircraft configurations.

CONCLUSIONS

Wind-tunnel tests have been conducted at Mach numbers of 0.85, 0.88, and 0.90 to determine the aerodynamic load distribution for the 39° swept-wing configuration of a variable-wing-sweep fighter airplane with a NASA supercritical airfoil. Chordwise pressure distributions were measured at two wing stations. Also measured were the overall longitudinal aerodynamic force and moment characteristics and buffet characteristics. The major conclusions are as follows:



1. The chordwise pressure distributions generally showed rearward movement of the shock wave location with increasing angle of attack and Mach number up to the point at which flow separation at the trailing edge occurs. Further increases in angle of attack resulted in gradual forward movement of the shock wave and an accompanying expansion of the region of separated flow.

2. At high subsonic Mach numbers, caution must be exercised in interpreting a rapid decrease in the trailing-edge pressure coefficient at isolated locations as an indication of buffet onset for the supercritical wing.

Langley Research Center,
National Aeronautics and Space Administration,
Hampton, Va., August 26, 1974.



REFERENCES

1. Harris, Charles D.: Wind-Tunnel Investigation of Effects of Trailing-Edge Geometry on a NASA Supercritical Airfoil Section. NASA TM X-2336, 1971.
2. Harris, Charles D.; and Blackwell, James A., Jr.: Wind-Tunnel Investigation of Effects of Rear Upper Surface Modification on an NASA Supercritical Airfoil. NASA TM X-2454, 1972.
3. Harris, Charles D.: Aerodynamic Characteristics of Two NASA Supercritical Airfoils With Different Maximum Thicknesses. NASA TM X-2532, 1972.
4. Ayers, Theodore G.: A Wind-Tunnel Investigation of the Application of the NASA Supercritical Airfoil to a Variable-Wing-Sweep Fighter Airplane. NASA TM X-2759, 1973.
5. Schaefer, William T., Jr.: Characteristics of Major Active Wind Tunnels at the Langley Research Center. NASA TM X-1130, 1965.
6. Loving, Donald L.: Wind-Tunnel—Flight Correlation of Shock-Induced Separated Flow. NASA TN D-3580, 1966.
7. Blackwell, James A., Jr.: Preliminary Study of Effects of Reynolds Number and Boundary-Layer Transition Location on Shock-Induced Separation. NASA TN D-5003, 1969.
8. Loving, Donald L.; and Katzoff, S.: The Fluorescent-Oil Film Method and Other Techniques for Boundary-Layer Flow Visualization. NASA MEMO 3-17-59L, 1959.
9. Davis, Don D., Jr.; and Huston, Wilber B.: The Use of Wind Tunnels To Predict Flight Buffet Loads. NACA RM L57D25, 1957.
10. Ray, Edward J.: Techniques for Determining Buffet Onset. NASA TM X-2103, 1970.
11. Ayers, Theodore G.: Transonic Aerodynamic Characteristics of a Variable-Wing-Sweep Tactical Fighter Model - Phase 5. NASA TM X-1368, 1967.
12. Anon.: Supercritical Wing Technology - A Progress Report on Flight Evaluations. NASA SP-301, 1972.

TABLE I.- PRESSURE ORIFICE LOCATIONS

[Measured with $\Lambda = 26^\circ$]

x/c	
Upper surface	Lower surface
0.02	0.02
.06	.06
.15	.15
.30	.30
.45	.45
.55	.55
.65	.65
.75	.75
.85	.85
.94	.94
.98	.98
1.00	

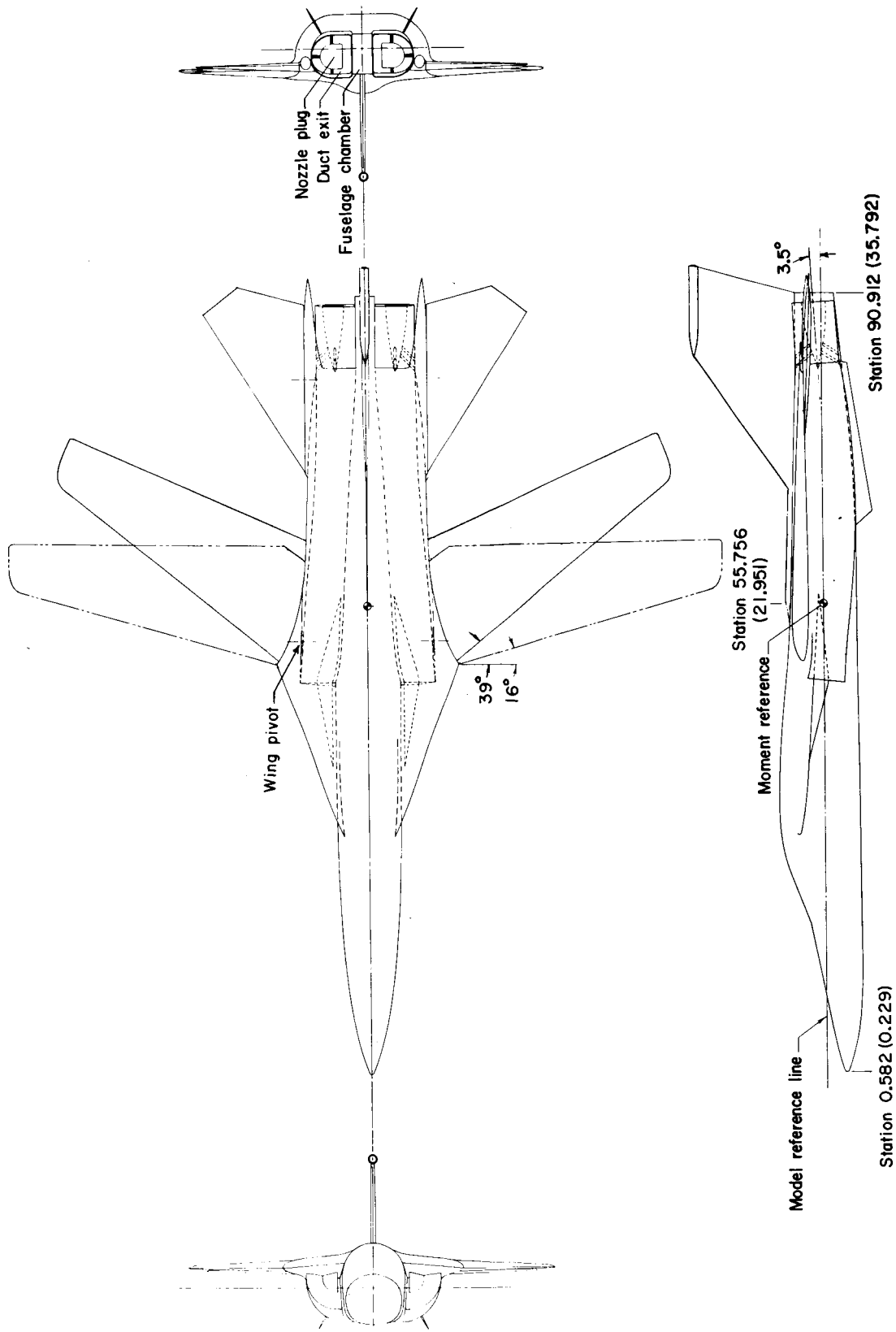
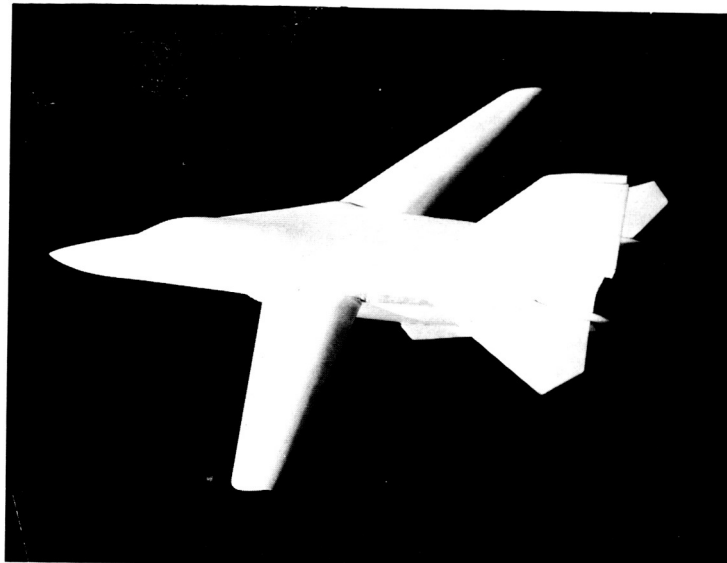
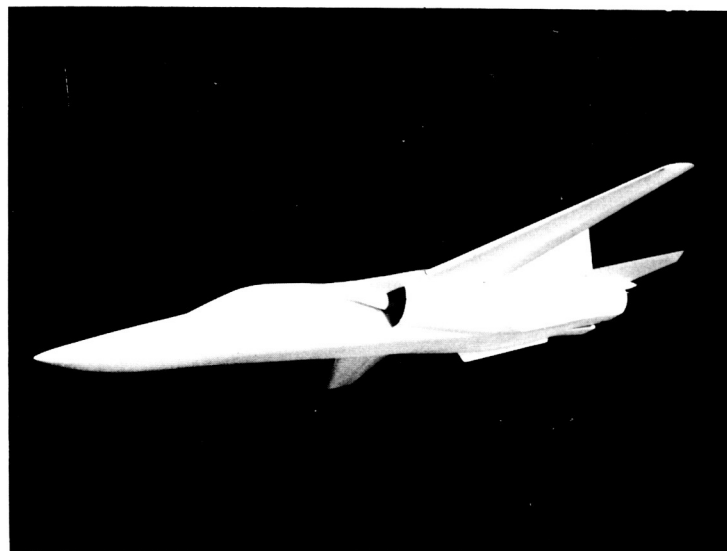


Figure 1.- General arrangement of 1/24-scale model variable-sweep fighter airplane. All dimensions are in cm (in.) unless otherwise noted.



L-68-3943



L-68-3942

Figure 2.- Variable-sweep fighter airplane with
supercritical wing. $\Lambda = 26^\circ$.

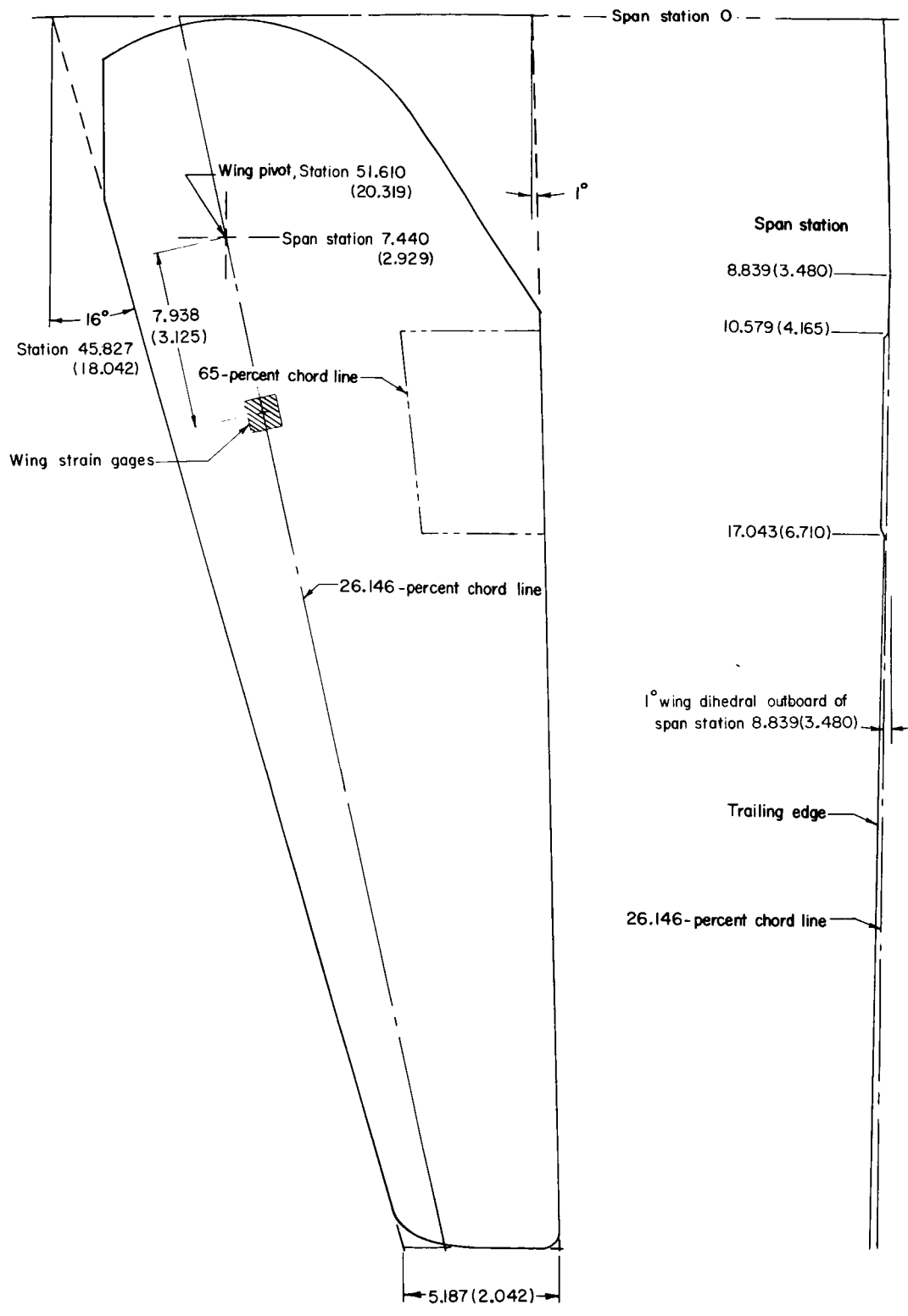


Figure 3.- Wing details. All linear dimensions are in cm (in.) unless otherwise noted.

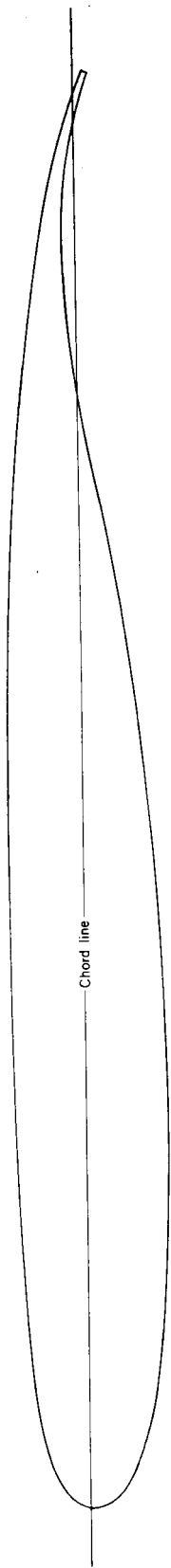


Figure 4.- Typical airfoil section.

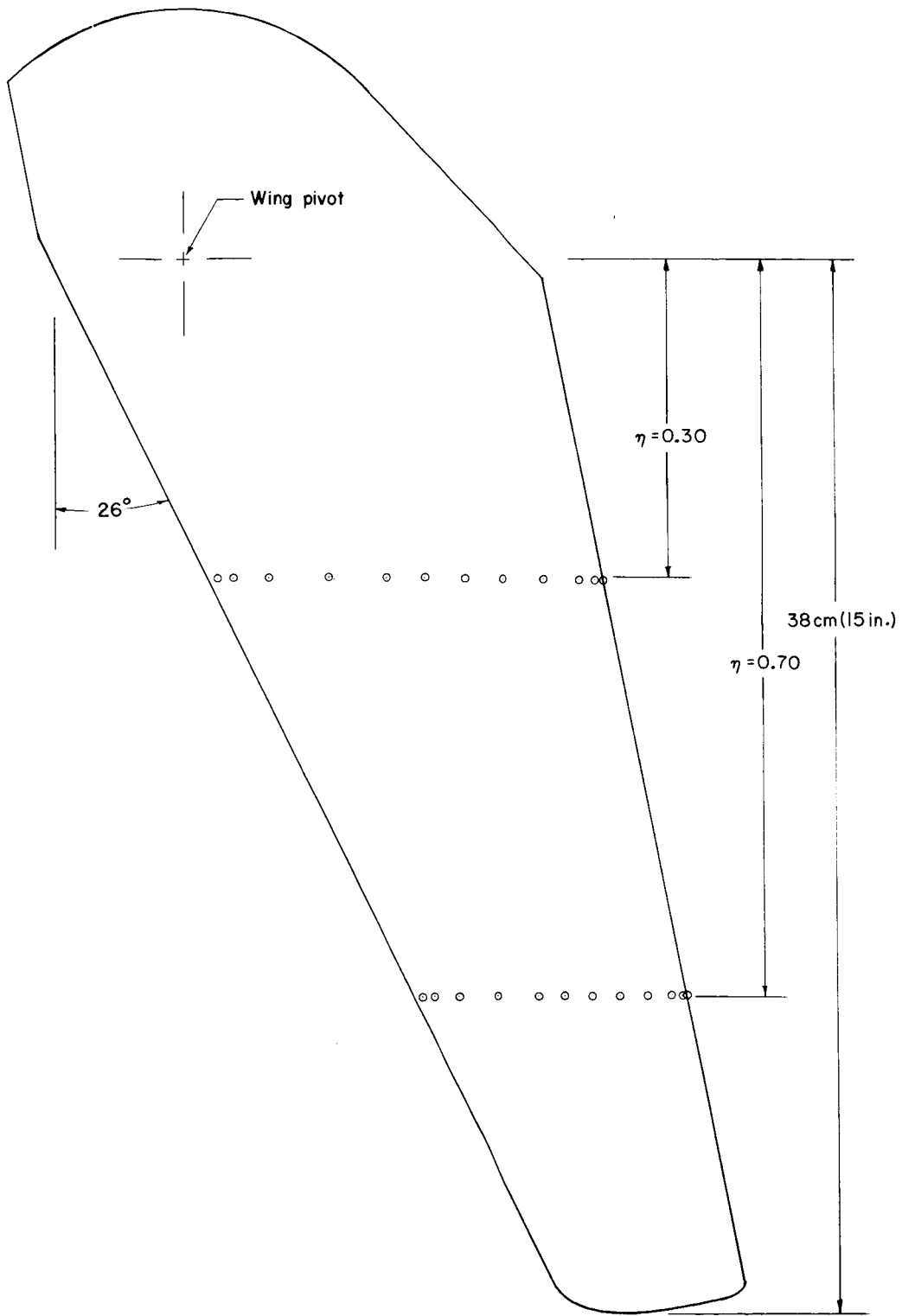
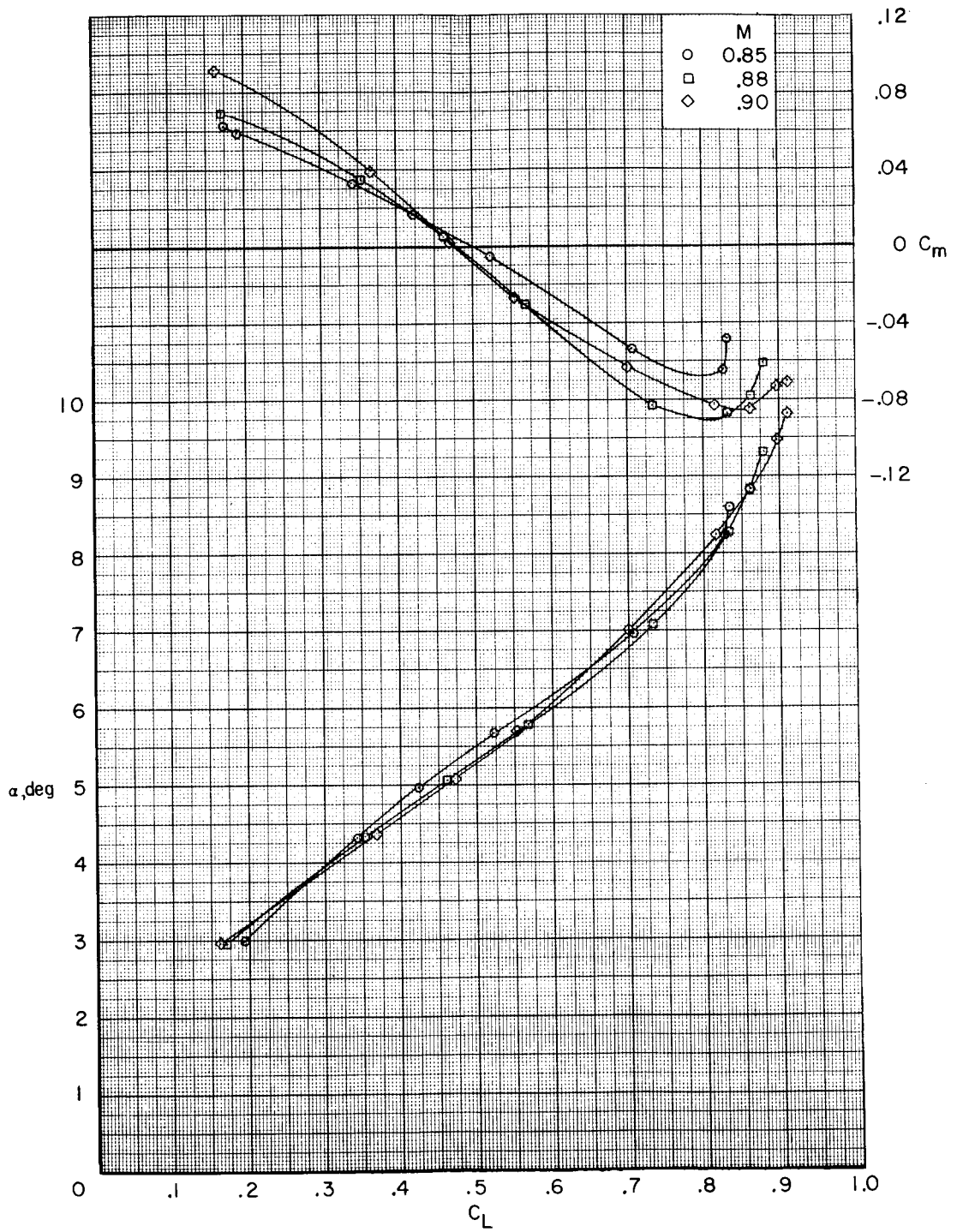
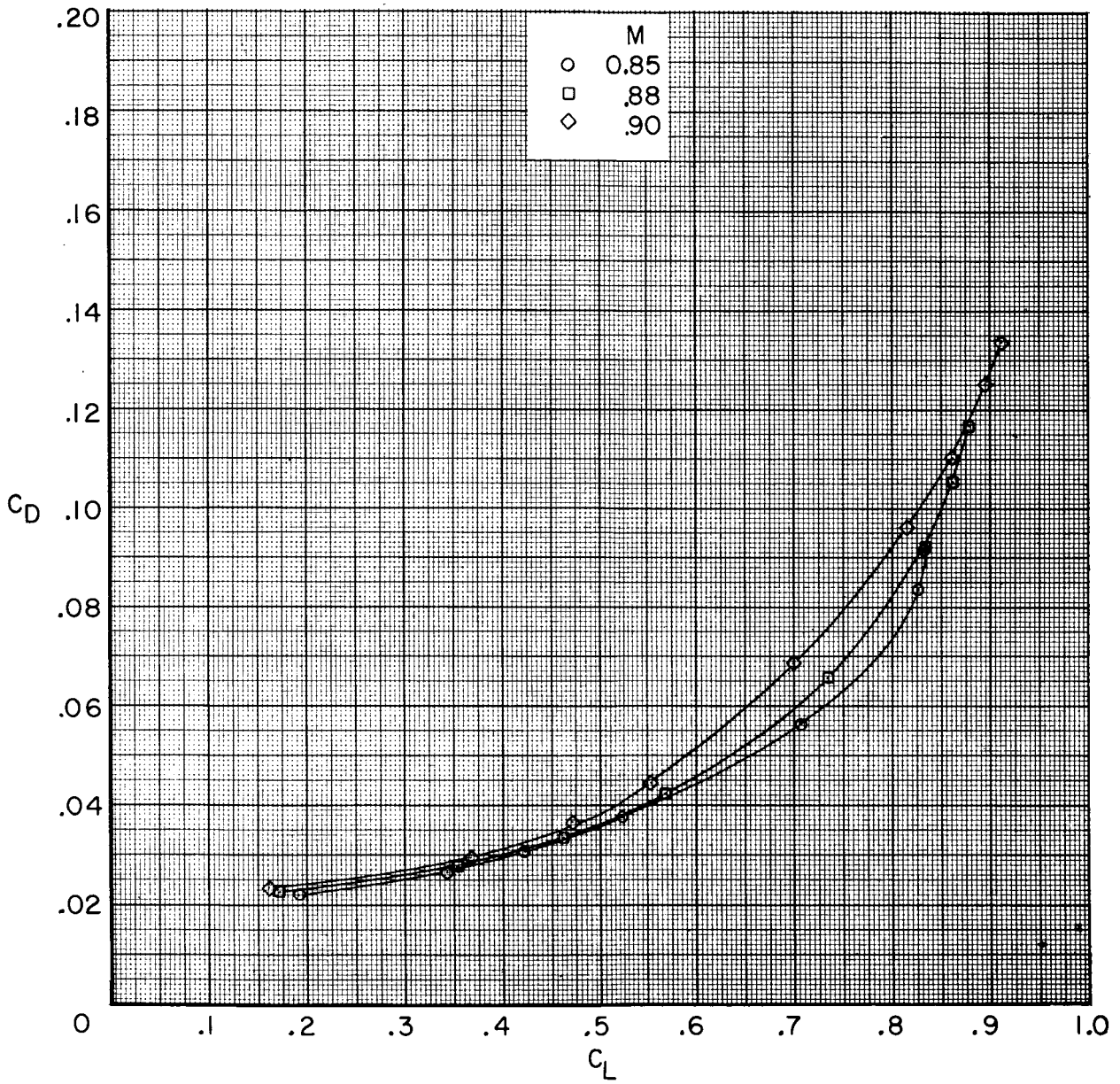


Figure 5.- Wing planform showing pressure orifice locations.



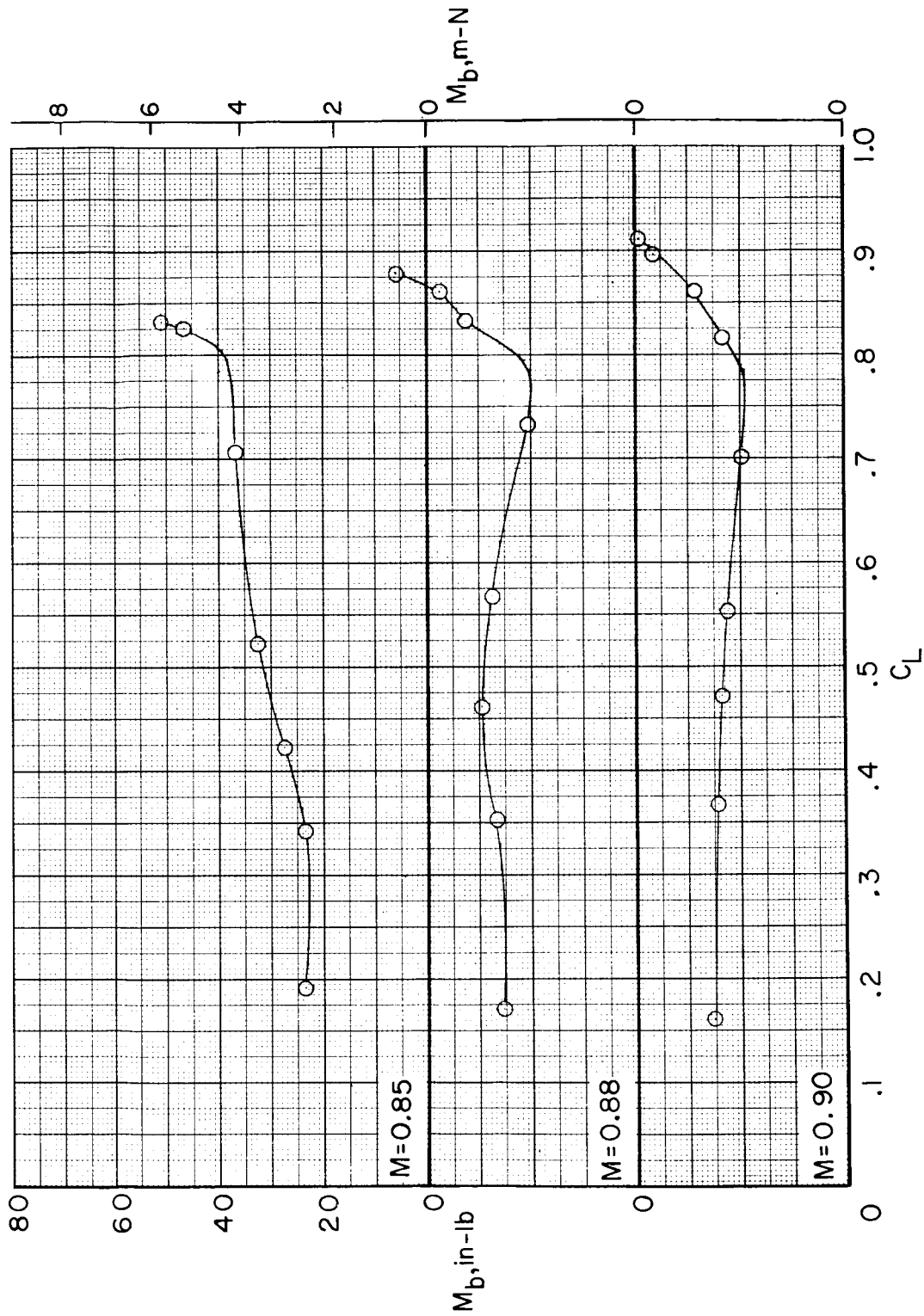
(a) α and C_m as functions of C_L .

Figure 6.- Aerodynamic characteristics of variable-wing-sweep fighter airplane with supercritical wing.



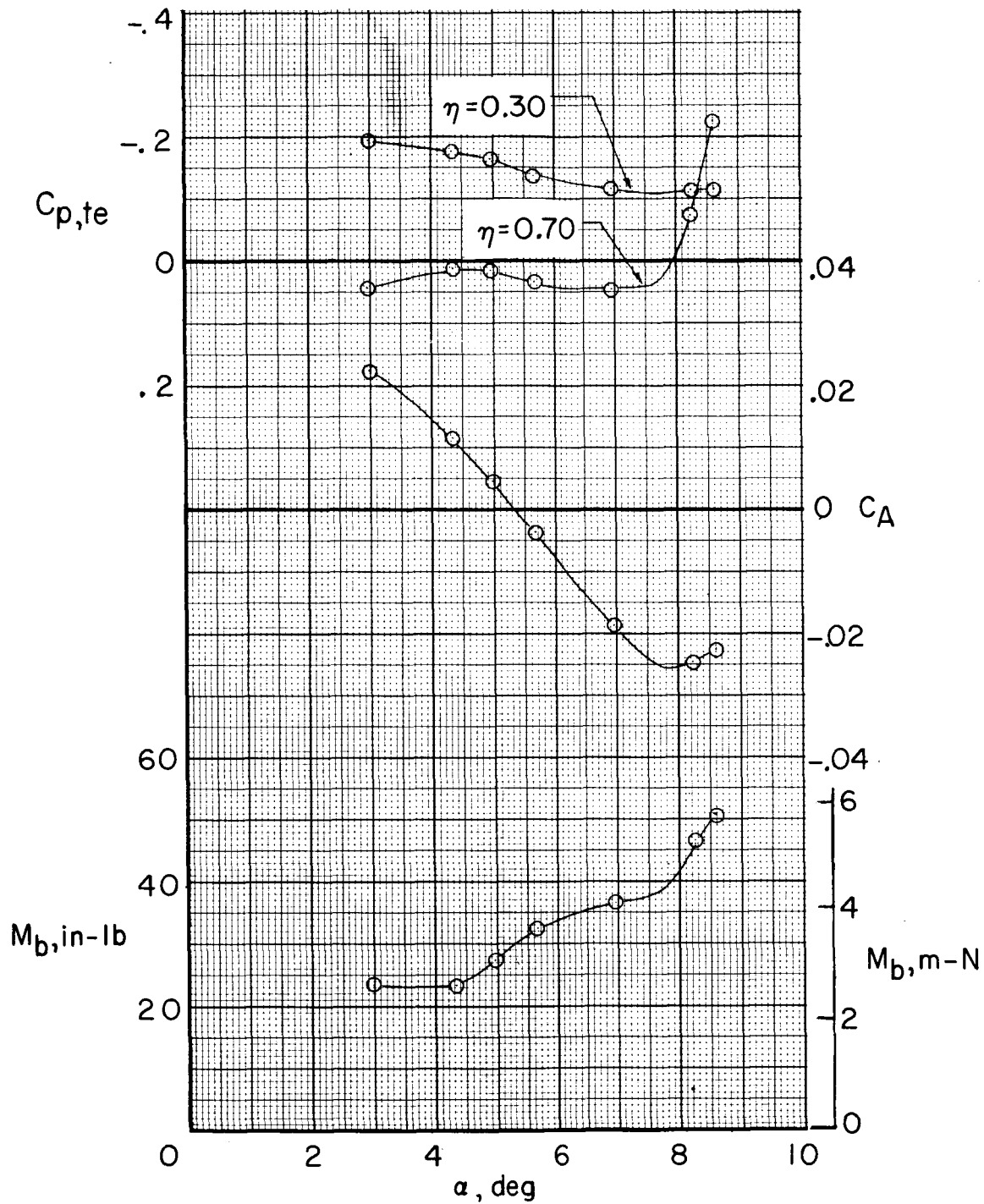
(b) C_D as a function of C_L .

Figure 6.- Continued.



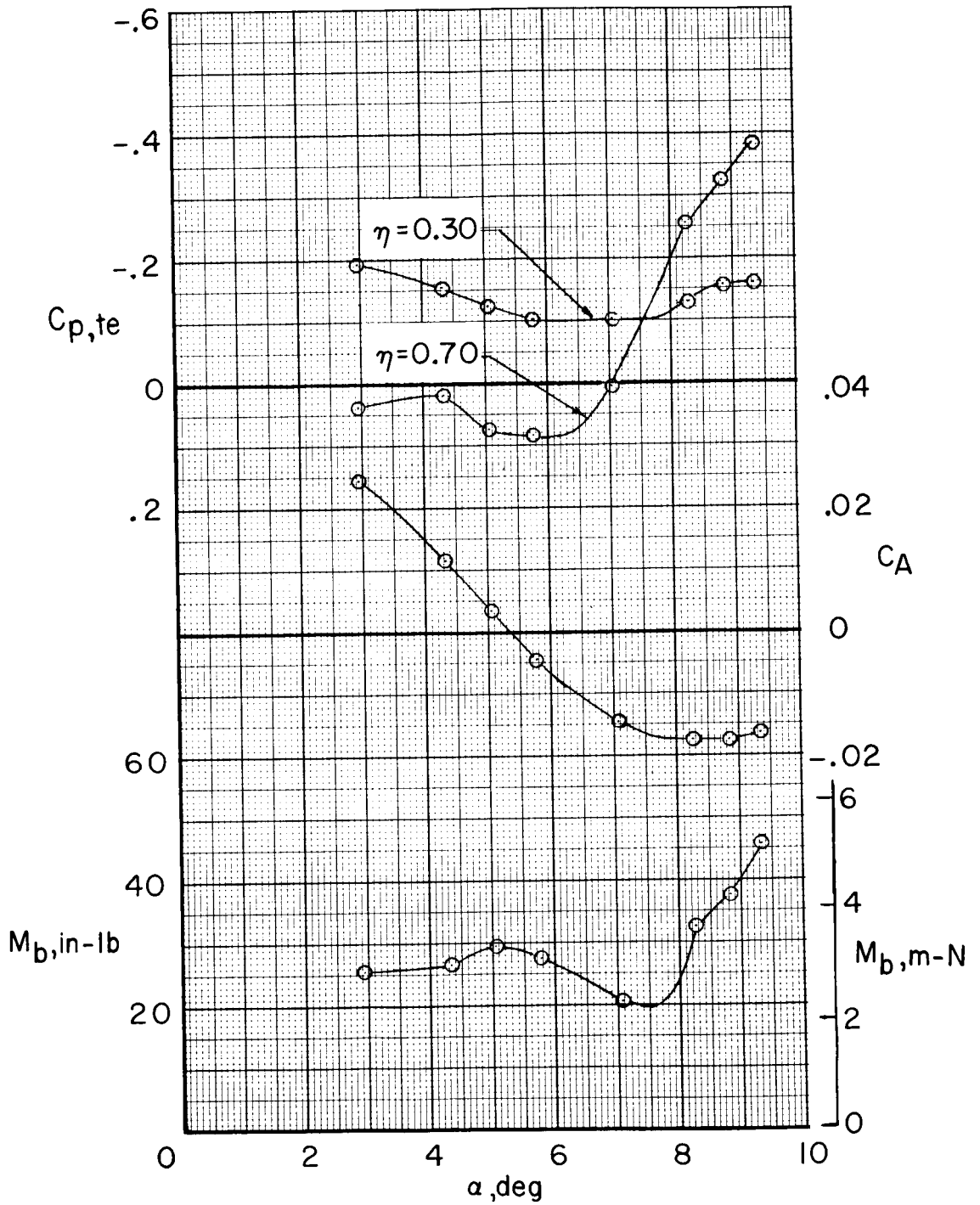
(c) M_b as a function of C_L .

Figure 6.- Concluded.



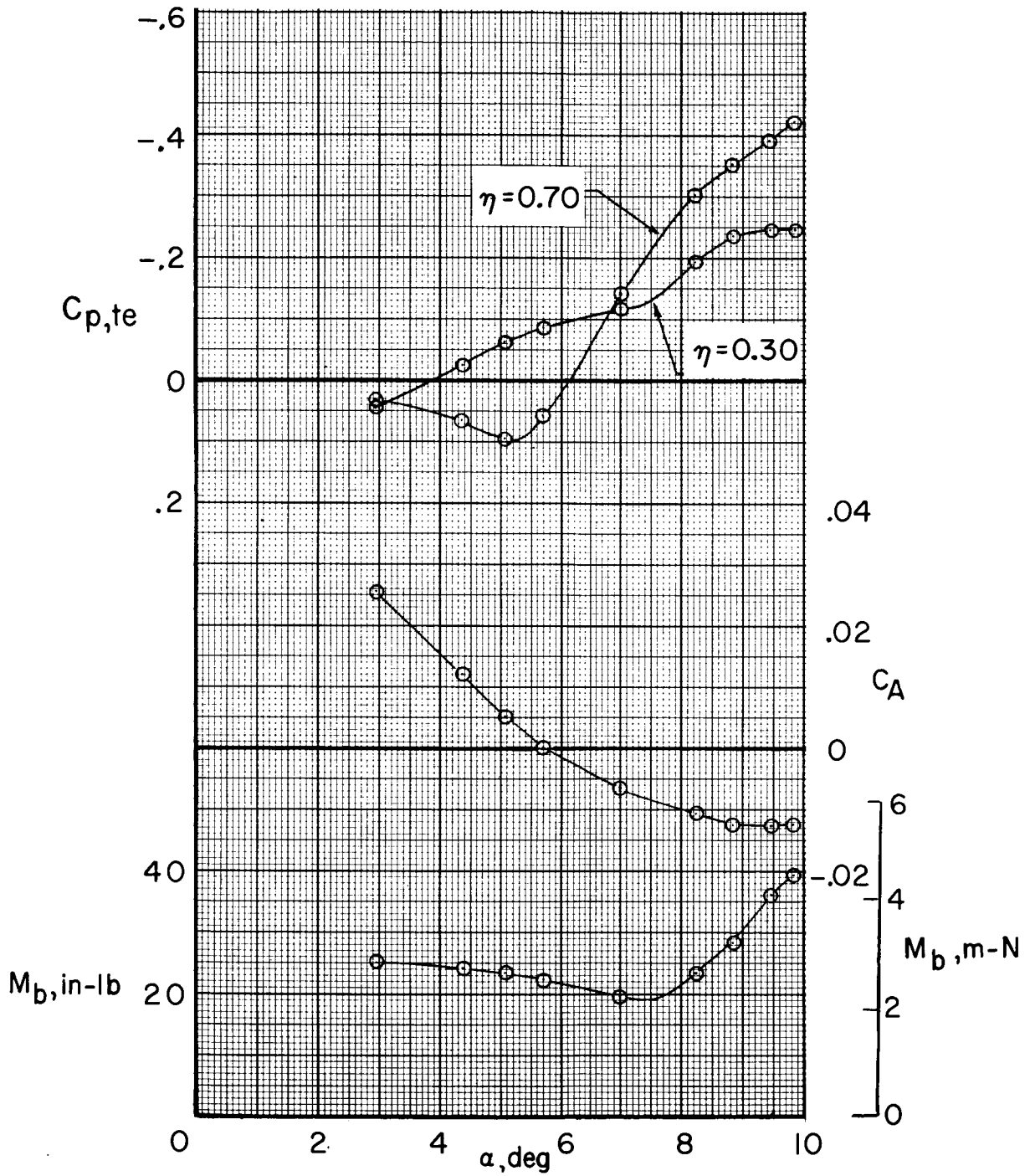
(a) $M = 0.85$.

Figure 7.- Variation with angle of attack of trailing-edge pressure coefficients, axial-force coefficients, and fluctuating wing-bending-moment characteristics.



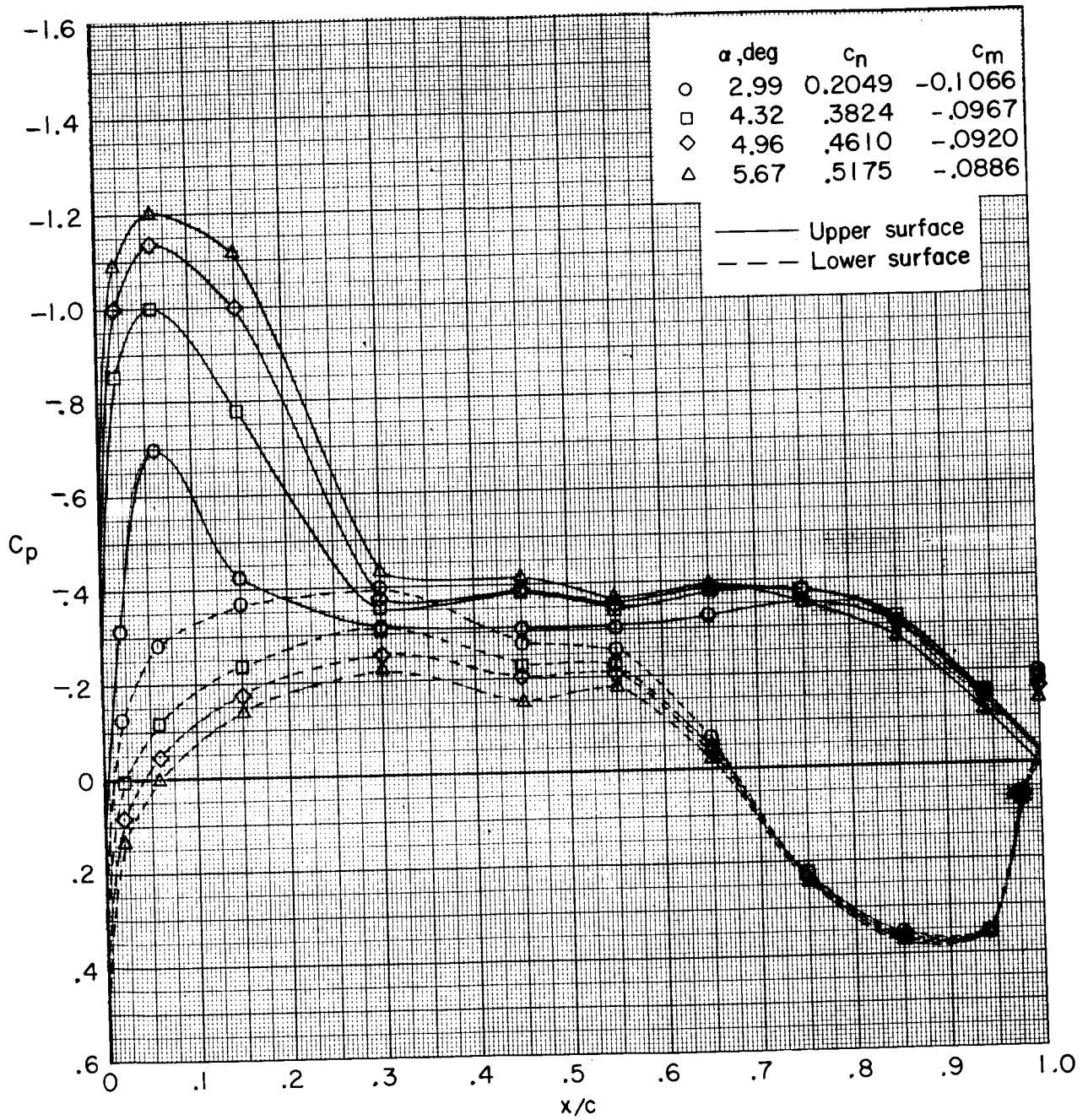
(b) $M = 0.88$.

Figure 7.- Continued.



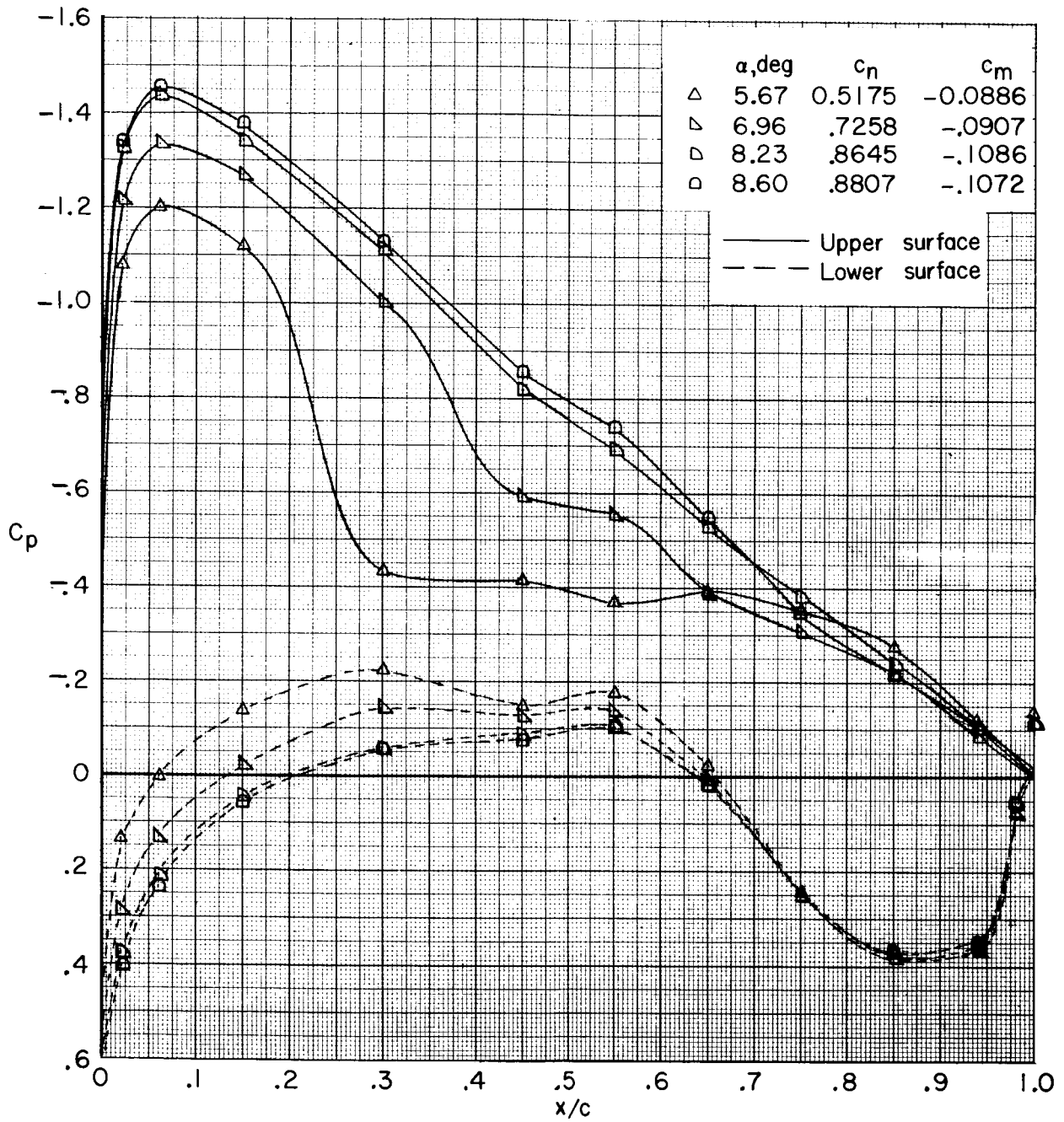
(c) $M = 0.90$.

Figure 7.- Concluded.



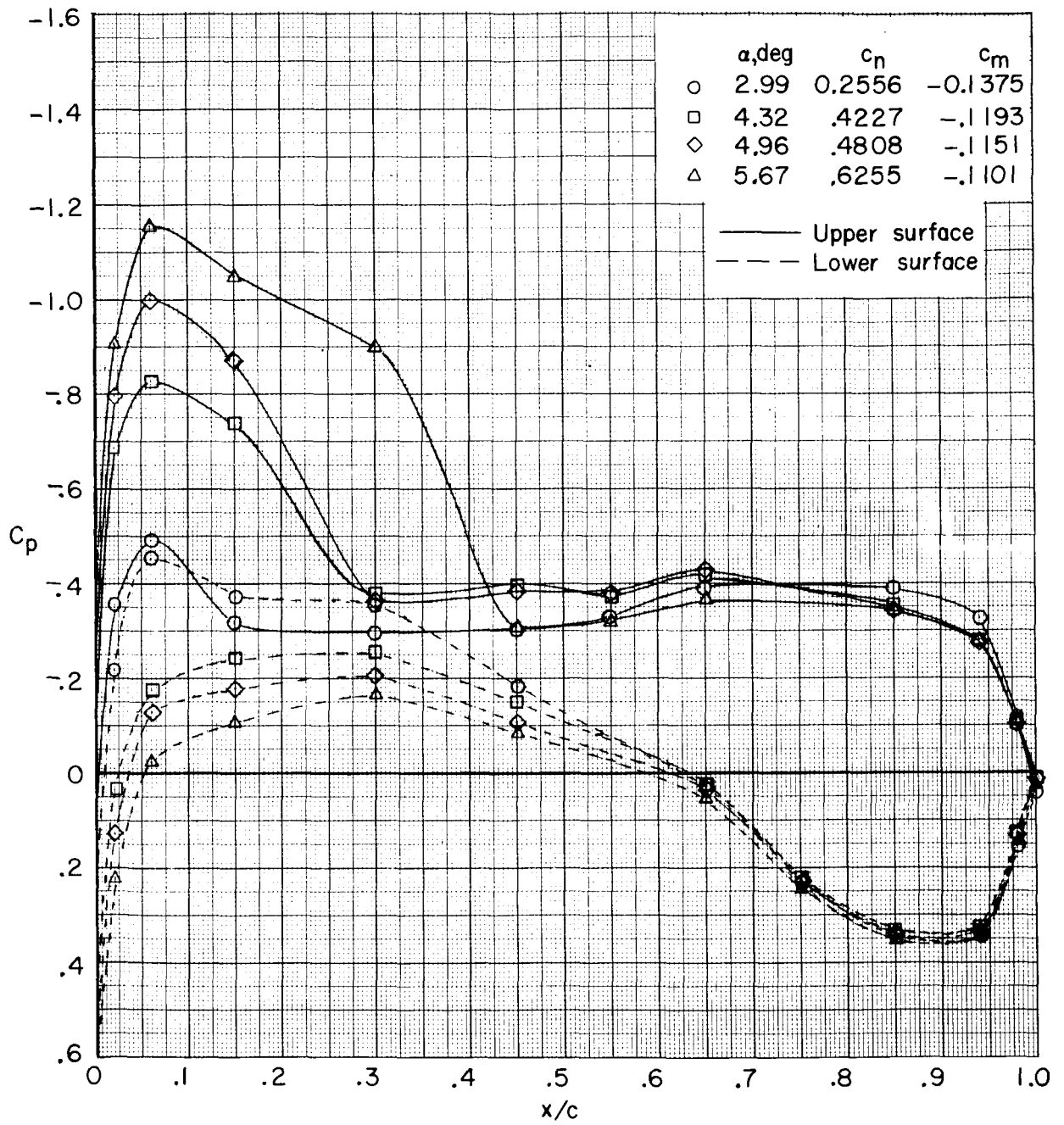
(a) $\eta = 0.3$; $\alpha = 2.99^\circ$ to 5.67° .

Figure 8.- Chordwise pressure distribution. $M = 0.85$.



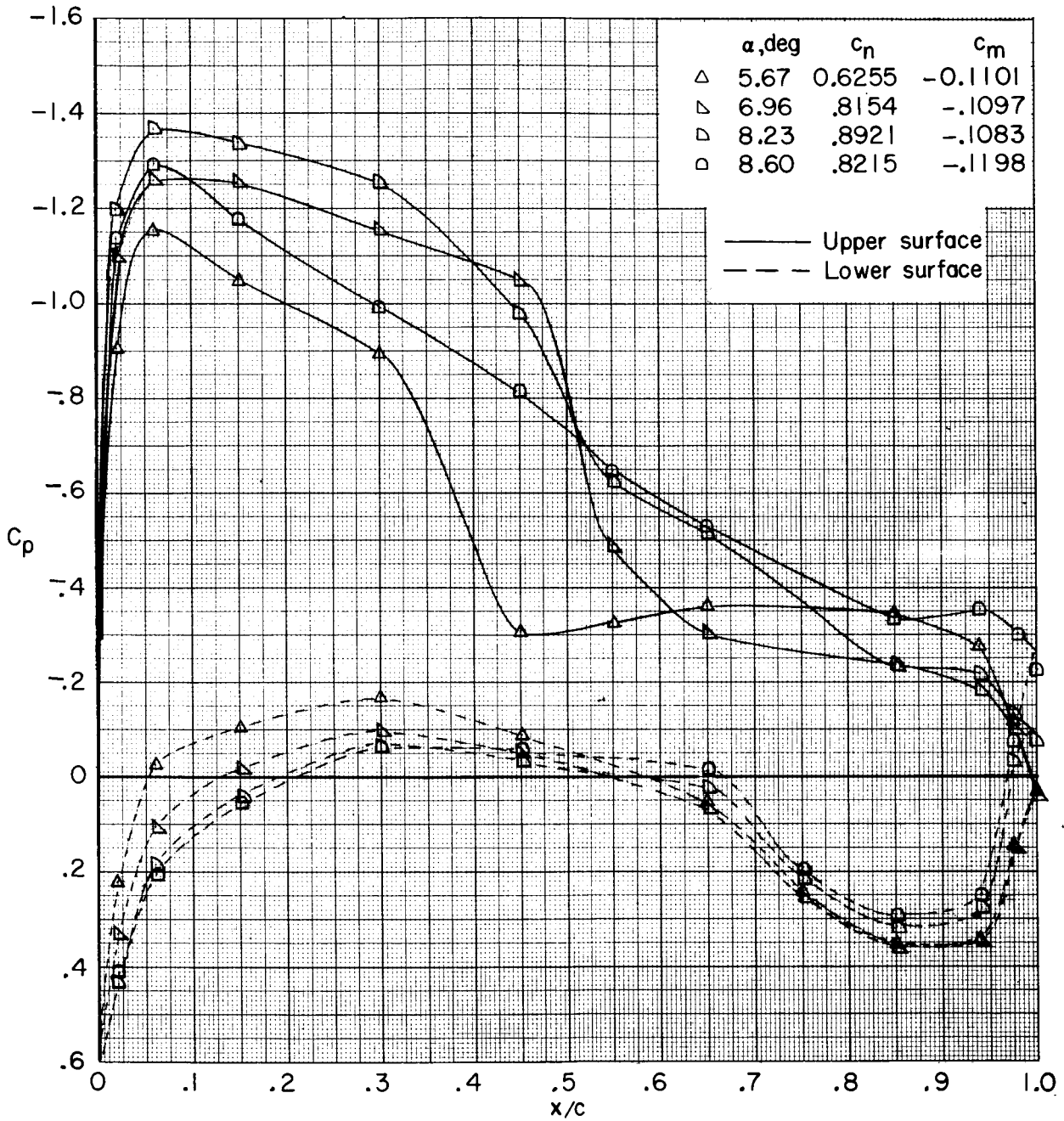
(a) $\eta = 0.3$; $\alpha = 5.67^\circ$ to 8.60° . Concluded.

Figure 8.- Continued.



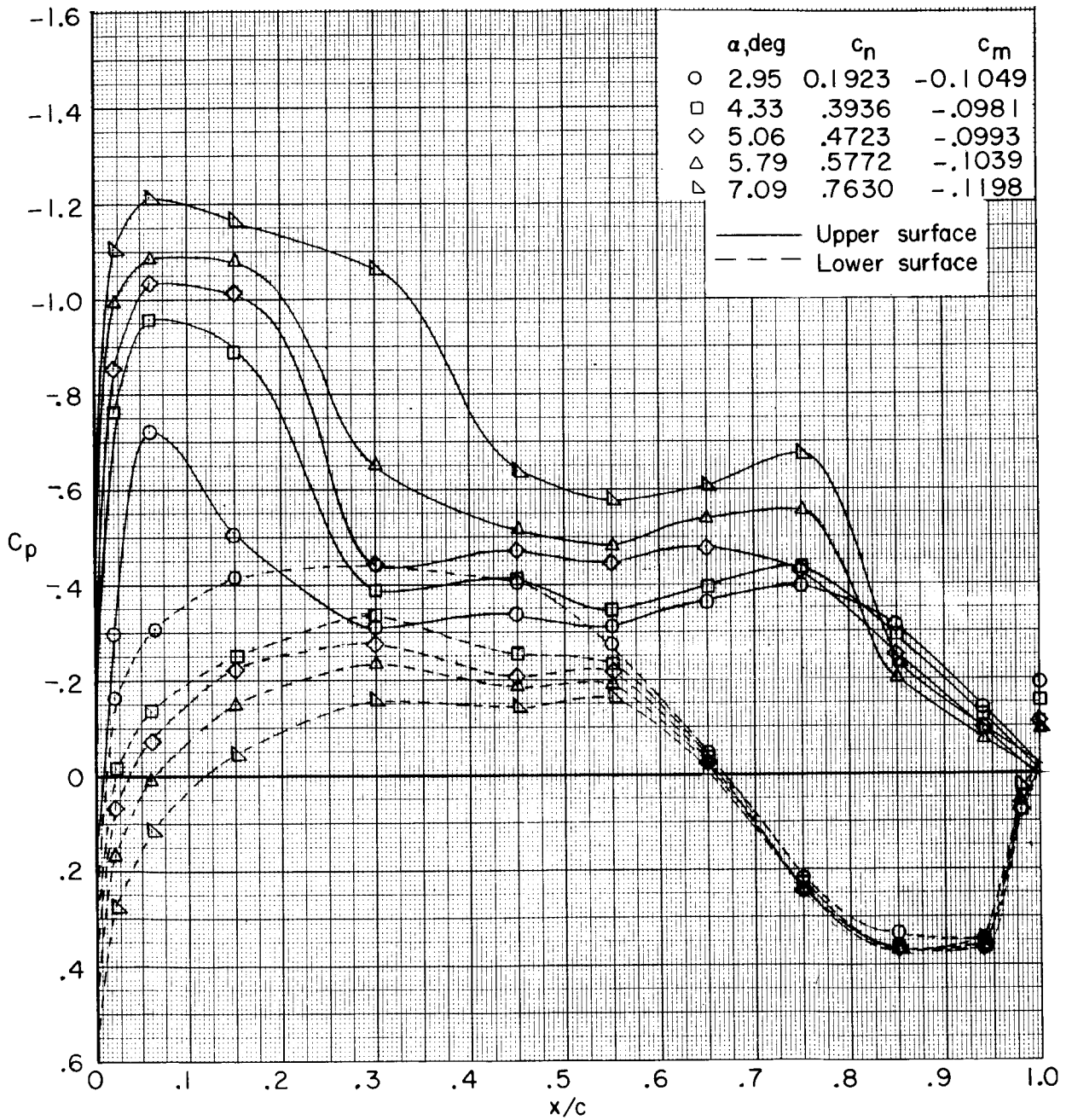
(b) $\eta = 0.7$; $\alpha = 2.99^\circ$ to 5.67° .

Figure 8.- Continued.



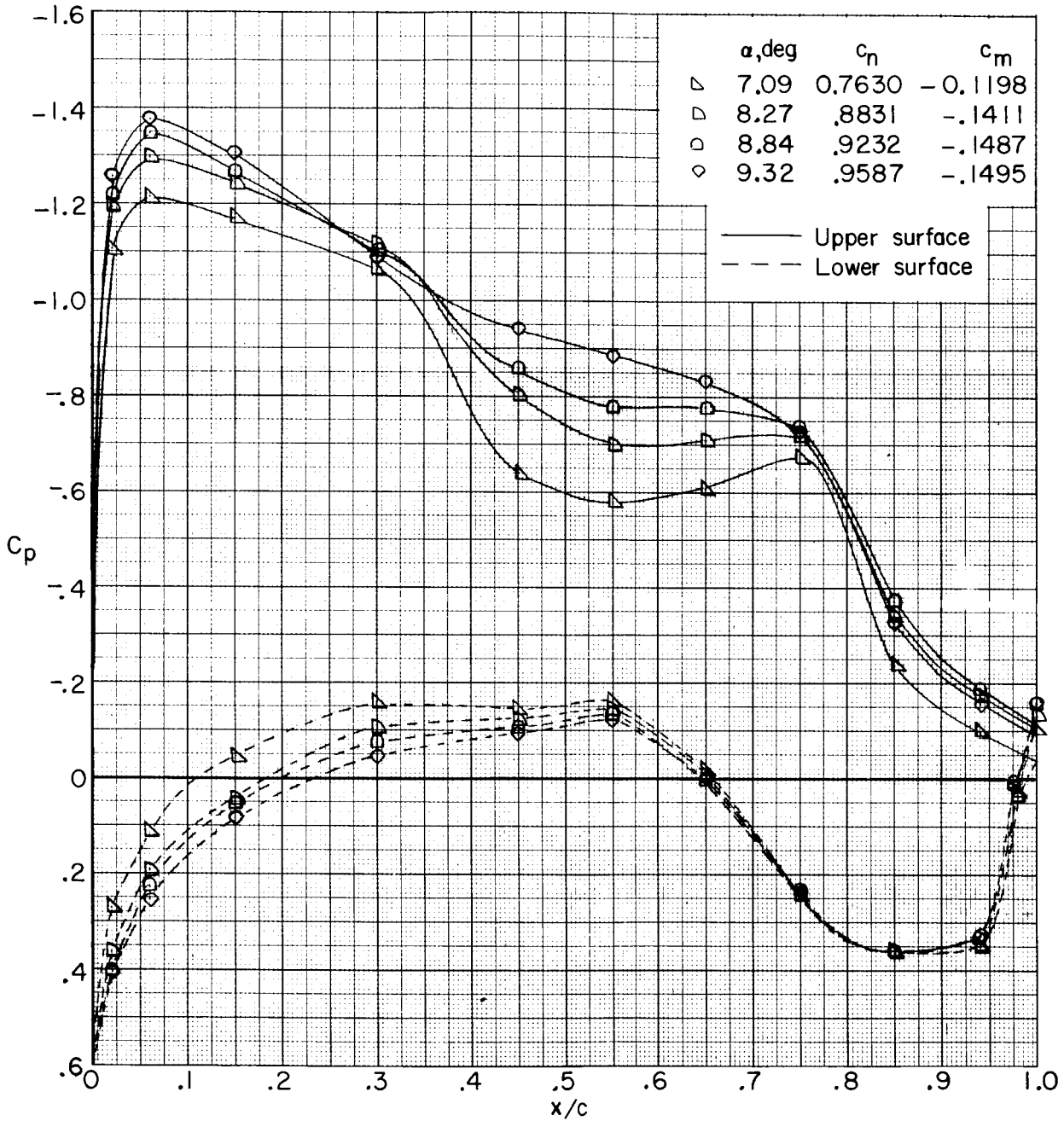
(b) $\eta = 0.7$; $\alpha = 5.67^\circ$ to 8.60° . Concluded.

Figure 8.- Concluded.



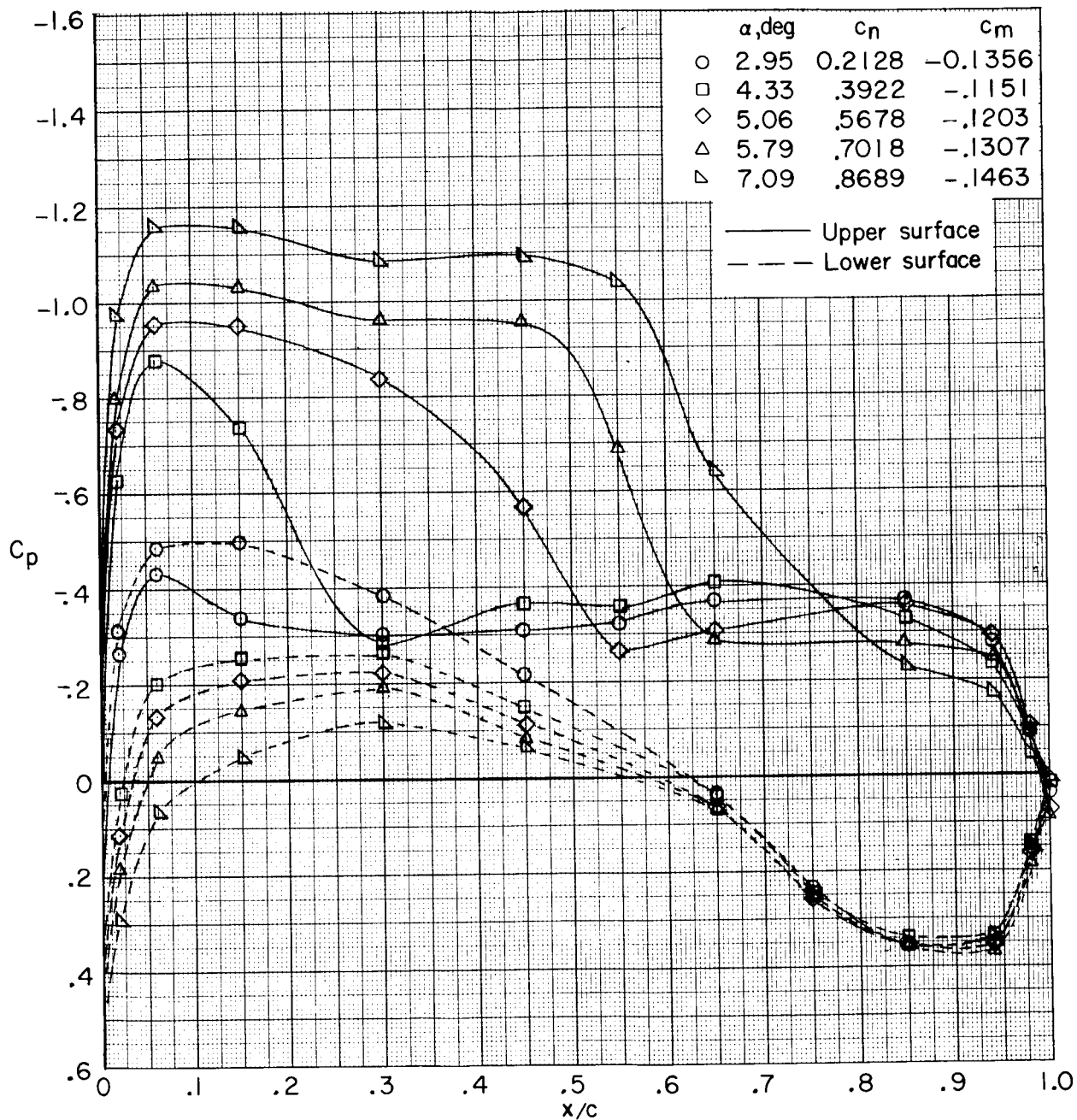
(a) $\eta = 0.3$; $\alpha = 2.95^\circ$ to 7.09° .

Figure 9.- Chordwise pressure distribution. $M = 0.88$.



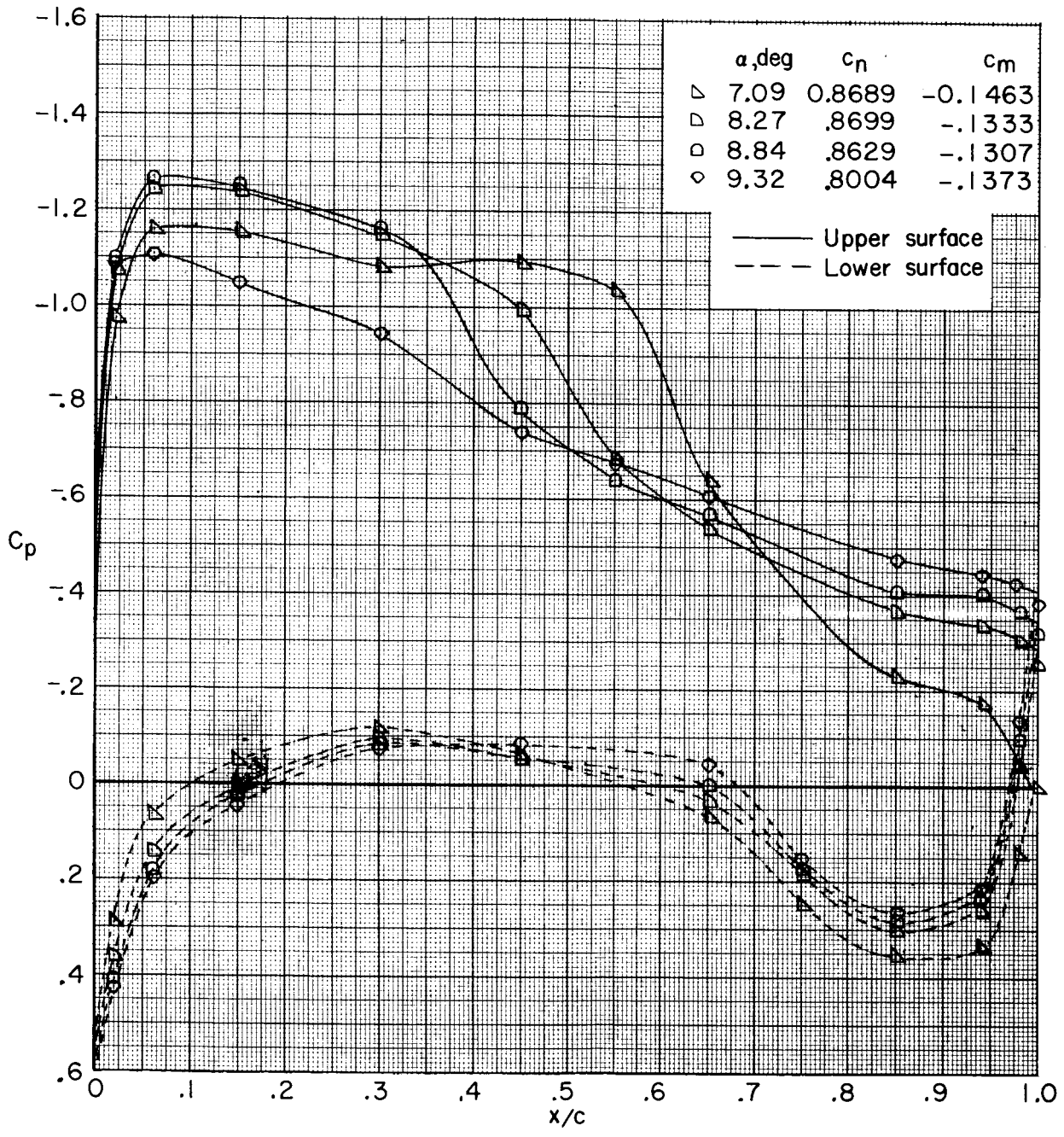
(a) $\eta = 0.3$; $\alpha = 7.09^\circ$ to 9.32° . Concluded.

Figure 9.- Continued.



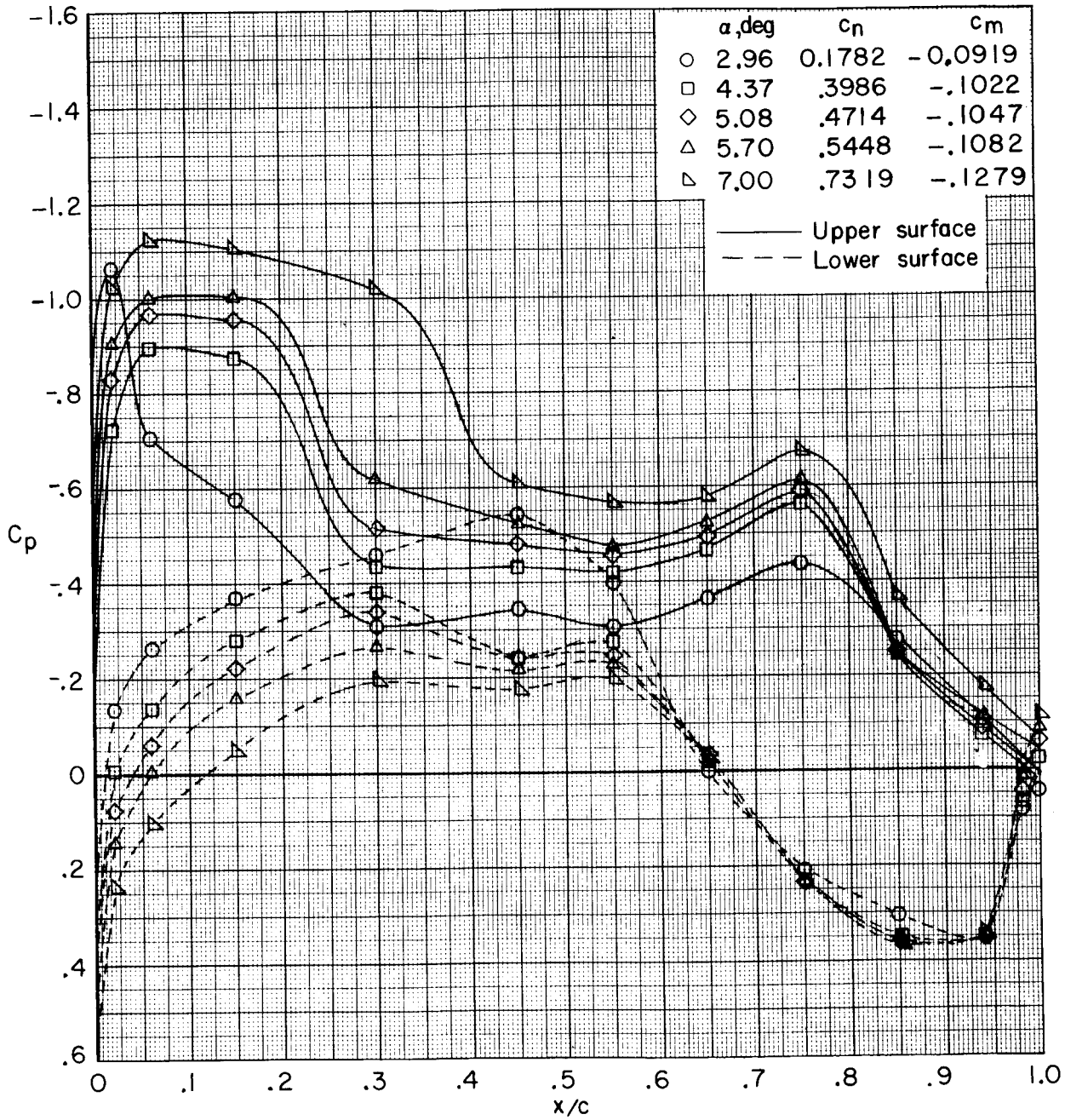
(b) $\eta = 0.7$; $\alpha = 2.95^\circ$ to 7.09° .

Figure 9.- Continued.



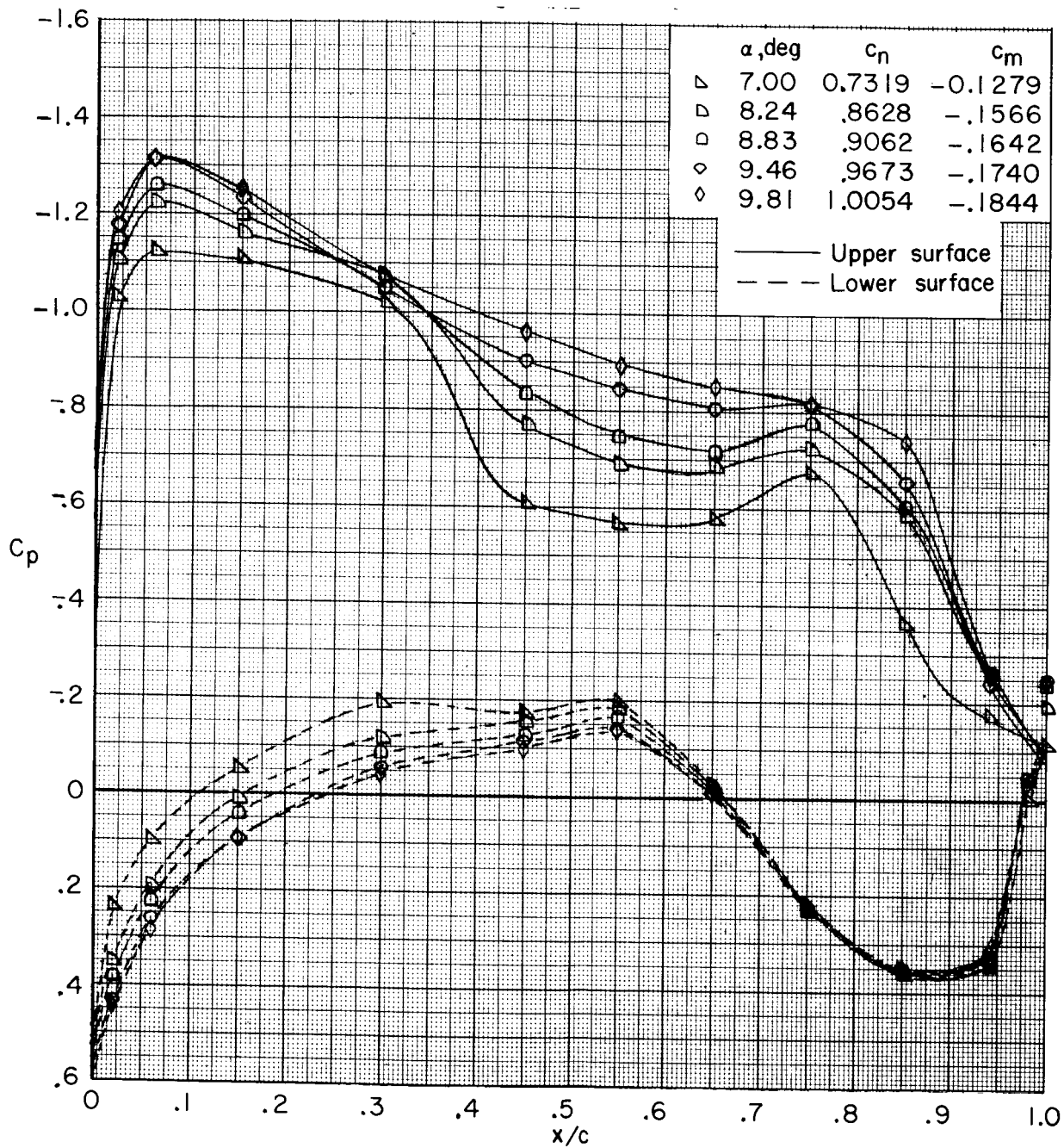
(b) $\eta = 0.7$; $\alpha = 7.09^\circ$ to 9.32° . Concluded.

Figure 9.- Concluded.



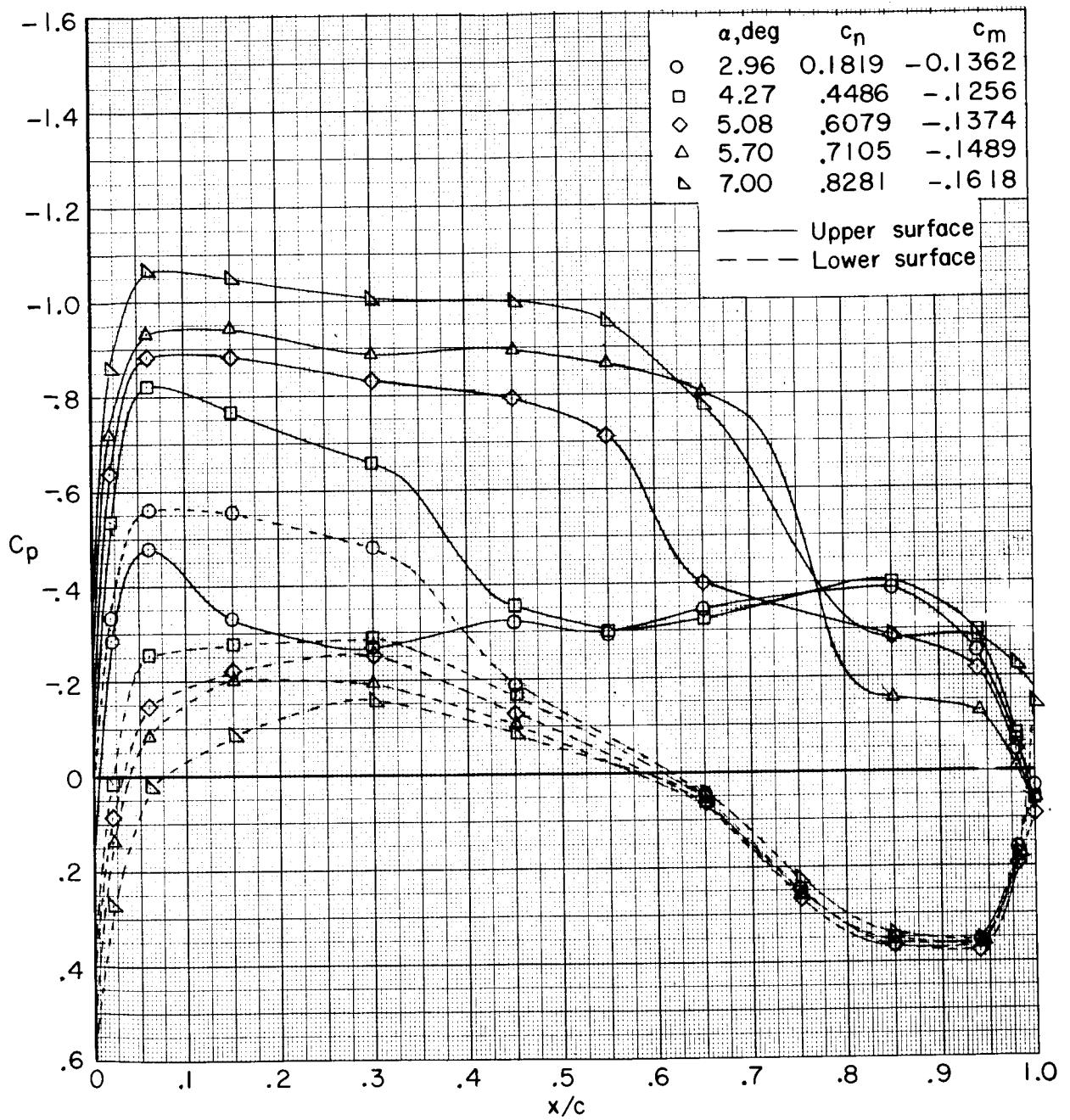
(a) $\eta = 0.3$; $\alpha = 2.96^\circ$ to 7.00° .

Figure 10.- Chordwise pressure distribution. $M = 0.90$.



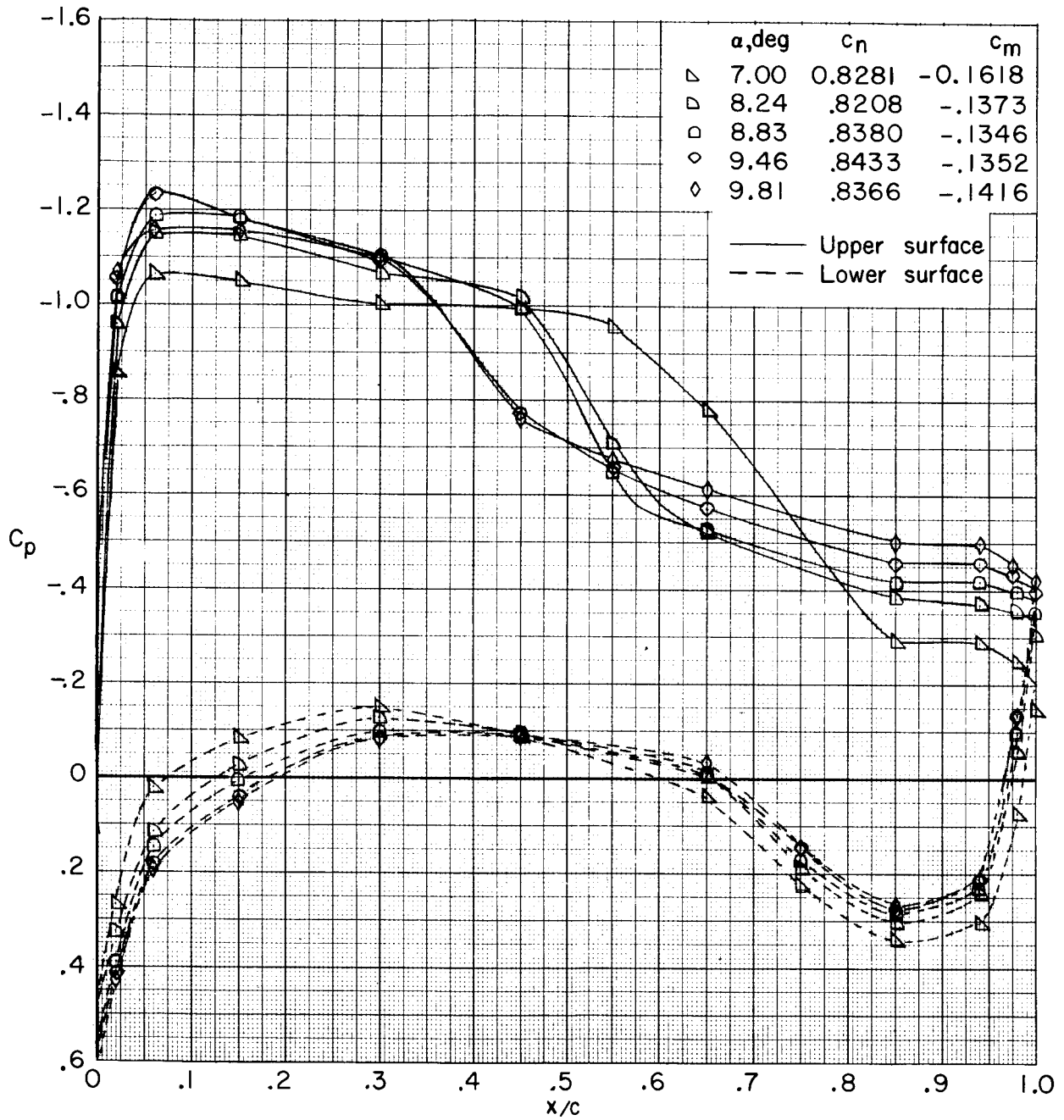
(a) $\eta = 0.3$; $\alpha = 7.00^\circ$ to 9.81° . Concluded.

Figure 10.- Continued.



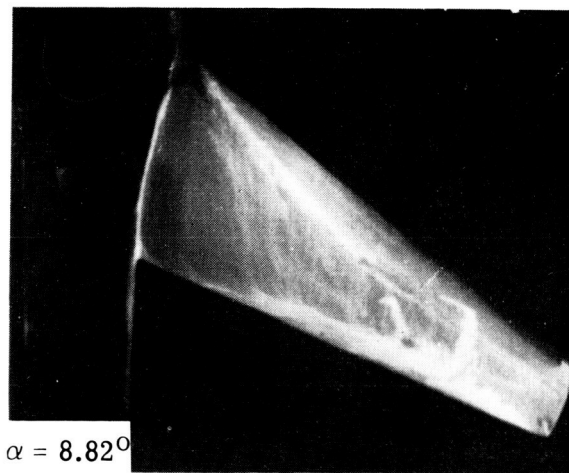
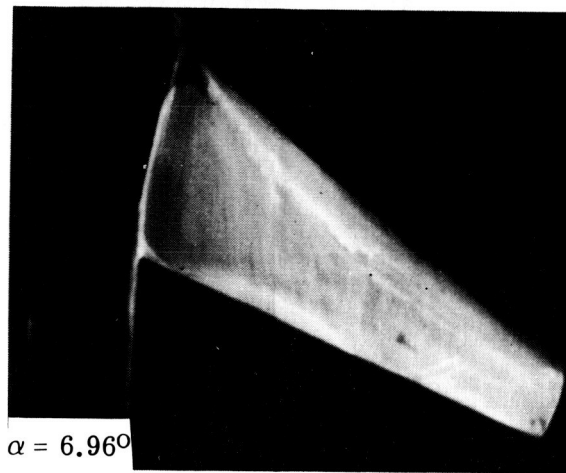
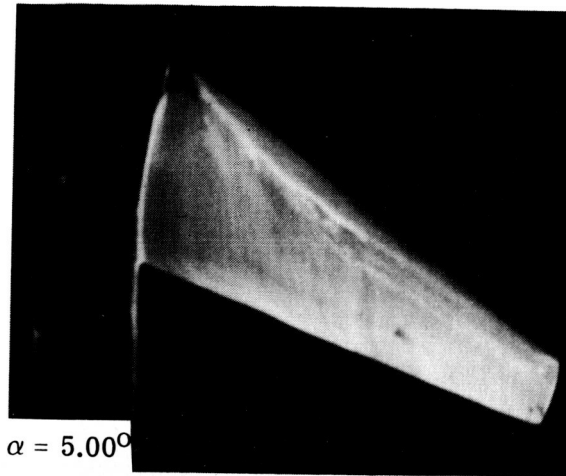
(b) $\eta = 0.7$; $\alpha = 2.96^\circ$ to 7.00° .

Figure 10.- Continued.



(b) $\eta = 0.7$; $\alpha = 7.00^\circ$ to 9.81° . Concluded.

Figure 10.- Concluded.



L-74-1152

Figure 11.- Oil flow photographs. $M = 0.90$.

1. Report No. NASA TM X-3095	2. Government Accession No.	3. Recipient's Catalog No.
4. Title and Subtitle WIND-TUNNEL INVESTIGATION OF AERODYNAMIC LOAD DISTRIBUTION ON A VARIABLE-WING-SWEEP FIGHTER AIRPLANE WITH A NASA SUPERCRITICAL AIRFOIL (U)	5. Report Date October 1974	6. Performing Organization Code
	8. Performing Organization Report No. L-9146	10. Work Unit No. 760-17-01-01
7. Author(s) James B. Hallissy and Charles D. Harris	11. Contract or Grant No.	13. Type of Report and Period Covered Technical Memorandum
9. Performing Organization Name and Address NASA Langley Research Center Hampton, Va. 23665	14. Sponsoring Agency Code	
	12. Sponsoring Agency Name and Address National Aeronautics and Space Administration Washington, D.C. 20546	
15. Supplementary Notes		
16. Abstract <p>Wind-tunnel tests have been conducted at Mach numbers of 0.85, 0.88, and 0.90 to determine the aerodynamic load distribution for the 39° swept-wing configuration of a variable-wing-sweep fighter airplane with a NASA supercritical airfoil. Chordwise pressure distributions were measured at two wing stations. Also measured were the overall longitudinal aerodynamic force and moment characteristics and the buffet characteristics. The analysis indicates that localized regions of shock-induced flow separation may exist on the rearward portions of the supercritical wing at high subsonic speeds, and caution must be exercised in the prediction of buffet onset when using variations in trailing-edge pressure coefficients at isolated locations.</p> <p style="text-align: center;">CLASSIFICATION CHANGE</p> <p style="text-align: center;">To UNCLASSIFIED</p> <p style="text-align: center;">By authority of <u>NASA HDA. T.D. 77-163</u> Changed by <u>L. Shirley</u> Date <u>6-15-76</u> Classified Document Master Control Station, NASA Scientific and Technical Information Facility</p>		
17. Key Words (Suggested by Author(s)) Load distribution NASA supercritical airfoil		
19. Security Classif. (of this report) Confidential	20. Security Unc	
"NATIONAL SECURITY INFORMATION" Unauthorized Disclosure Subject to Criminal Sanctions.		